# Combining experimental and modelling approaches to monitor the transport of an artificial tracer through the hyporheic zone

Clémence Houzé, Véronique Durand, Claude Mügler, Marc Pessel, Gaël Monvoisin, Christelle Courbet, Camille Noûs

## To cite this version:

Clémence Houzé, Véronique Durand, Claude Mügler, Marc Pessel, Gaël Monvoisin, et al.. Combining experimental and modelling approaches to monitor the transport of an artificial tracer through the hyporheic zone. Hydrological Processes, 2022, 36 (2), 10.1002/hyp.14498 . hal-03604096

HAL Id: hal-03604096
https://hal.science/hal-03604096v1

Submitted on 12 Apr 2022

# Combining experimental and modelling approaches to monitor the transport of an artificial tracer through the hyporheic zone

## Running head: Experiments and modelling to study the transport within the HZ

*Clémence Houzé*[a1], *Véronique Durand*[a]*, *Claude Mügler*[b], *Marc Pessel*[a], *Gaël Monvoisin*[a], *Christelle Courbet*[c], *Camille Noûs*[d]

[a]Laboratoire GEOPS, UMR 8148 Univ. Paris-Saclay-CNRS, Bât. 504, 91405 Orsay Cedex, France

[b]Laboratoire des Sciences du Climat et de l'Environnement, UMR 8212 CEA-CNRS-UVSQ, Orme des Merisiers, 91191 Gif-sur-Yvette Cedex, France

[c]IRSN, PSE-ENV/SEDRE/LELI, BP 17, 92262 Fontenay-aux-Roses CEDEX, France

[d]Laboratoire Cogitamus, Univ. Paris-Saclay-CNRS, Bât. 504, 91405 Orsay Cedex, France

*Corresponding author: veronique.durand@universite-paris-saclay.fr

## Acknowledgements

The authors would like to thank the Essonne River syndicate (SIARCE) and particularly M. Sahaghian for permitting these experiments on the Essonne River and supporting their implementation. This work received support from the French national program EC2CO-Biohefect/Ecodyn/Dril/MicrobiEn (DynamelZH). We are grateful to the two anonymous reviewers for their most constructive comments that helped us to make substantial improvements to the manuscript.

---

[1] Now at SIARCE, 58 rue Fernand Laguide, 91100 Corbeil-Essonnes, France

**Keywords**

Hyporheic zone, artificial tracer transport, time-lapse Electrical Resistivity Tomography (ERT), modelling.

## Abstract

In order to advance methodologies used in the investigation of Hyporheic Zone (HZ) mixing processes, this paper combines experimental and modelling tools to follow a tracer injected into the river and infiltrating into the HZ. A highly concentrated sodium chloride solution was injected into the river; (i) the river conductivity, (ii) the riverbed resistivity by Electrical Resistivity Tomography (ERT), and (iii) vertically distributed chloride concentrations within the HZ were monitored. Both ERT and concentration measurements showed an infiltration depth of the tracer of 35 cm, and a partial recovery after injection, which was faster within the superficial layer that was found to be more resistive according to the ERT initial image. The modelling approach used the HydroGeoSphere code to model the coupling between river surface flows and HZ groundwater flows and transport processes. The model set up involved a 50 cm high existing riverbed step, a vertical contrast in HZ saturated hydraulic conductivity and the aquifer discharge flux. Fitting the vertical chloride profile, the adjusted values were $5 \times 10^{-2}$ m.s$^{-1}$ for the saturated hydraulic conductivity of the first highly permeable layer below the riverbed, and $4 \times 10^{-6}$ m.s$^{-1}$ for the aquifer discharge flux. The bottom layer saturated hydraulic conductivity was found to be at least ten times lower than the value within the first layer. Numerical simulations showed that the two main parameters controlling the mixing within the HZ were the groundwater discharge and the saturated hydraulic conductivity first sediment layer of the riverbed. The riverbed step was found to be less significant here compared to these two parameters. The combination of experimental

and modelling tools allowed us to quantify the aquifer discharge flux, which is complicated to investigate in the field without any model. Results of this study showed that combining modelling with ERT and vertically distributed chloride sampling allows the quantification of the main factors controlling the hyporheic exchange.

## 1-Introduction

Surface water-groundwater interactions help to preserve water quality and biodiversity in streams (Buss *et al.*, 2009). These interactions take place in the hyporheic zone (HZ), which is defined as the transition zone between the stream channel and the adjacent groundwater that contains some proportions of stream water (Harvey and Bencala, 1993). Despite a recent increase in studies interested in hyporheic mixing fluxes (Ward, 2016), there is a need to improve the approaches on this subject (Lewandowski *et al.*, 2019).

The major parameters that are acknowledged to control the mixing between the groundwater and the surface water within the HZ differ depending on the type of methodology chosen (Ward and Packman, 2019). A clear distinction in the existing literature can be made between theoretical and experimental studies. We will explore both types here.

In the first type of study, mathematical analysis focused on the influence of bed forms on bed-stream exchanges (e.g. Cardenas and Wilson (2007), Elliott and Brooks (1997)). Models based on physical laws were then used extensively to try to identify the main factors contributing to these exchanges. Hester and Doyle’s (2008) modelling indicated that sediment hydraulic conductivity and groundwater discharge rate towards the stream were the most important factors influencing hyporheic exchange, followed by structure type, depth to bedrock, and channel slope. These results were in agreement with modelling studies that showed that the discharge of deep groundwater into the surface water column reduced the spatial extent of the bedform-induced exchange zone (Cardenas and Wilson, 2006). The influence of sediment heterogeneity on HZ extension has also been investigated using numerical simulations. Sawyer and Cardenas (2009) showed that mixing depth and solute distributions in sediments were relatively insensitive to hydraulic conductivity heterogeneity. Recent simulations of hyporheic mixing in heterogeneous river beds have confirmed that a large upward groundwater flow, which offsets the effects of heterogeneity, is one of the main controlling factors of the mixing process (Su *et al.*, 2020). However, most numerical studies are based on simplistic assumptions and may not reflect the complexity found in nature. For example, they may not capture phenomenon such as natural riverbeds with small- and large-scale morphological variations, complex hydraulic conductivity distributions of natural sediment with more or less permeable inclusions and/or layers, and natural temporal variations in river and groundwater hydrology. (Su *et al.*, 2020) acknowledged that verification of their numerical results through field investigations would be necessary.

To overcome this issue, some authors used a combination of laboratory experimental systems and modelling approaches to study the hyporheic zone. Flume experiments and numerical simulations of hyporheic exchange in riverbeds coupled with pool-riffle morphology showed that the 3-D morphology of the pool-riffle strongly influences the hyporheic flow (Tonina and Buffington, 2007). Flume experiments and numerical simulations were also used to investigate the effects of losing and gaining flow conditions on hyporheic exchange fluxes in a sandy rippled streambed (Fox *et al.*, 2014). Both experiments and modelling showed that the hyporheic exchange flux becomes smaller as the losing or gaining flux increases. However, all these experiments were performed in a laboratory with a well-calibrated small-scale flume system.

From theoretical studies, one can conclude that the main factors controlling the mixing within the HZ are: the aquifer discharge flux (Boano *et al.*, 2009, Cardenas and Wilson, 2006, Fox *et al.*, 2014); the riverbed sediments' hydraulic conductivity (Su *et al.*, 2020), and, to a lesser extent, geomorphologic factors within the river and the aquifer (Hester and Doyle, 2008). But are these theoretical results consistent with field experimental studies? One of the most common experimental methods for studying the hyporheic mixing fluxes is the tracer approach. The tracer can be injected directly into the riverbed sediments (Houzé *et al.*, 2017, Käser *et al.*, 2009), but this remains uncommon. The tracer is most often injected into the river (Castro and Hornberger, 1991, Harvey *et al.*, 1996, Kelleher *et al.*, 2019, Ward *et al.*, 2012, Ward *et al.*, 2019), and monitored downstream in the river, often within at least one piezometer, located either on the riverbank or below the riverbed, to quantify the river water infiltrated into the hyporheic zone. This type of studies is often combined with a Transient Storage Model (TSM) which explores the way the tracer can be retained and retrieved within and from the HZ (see Boano *et al.* (2014) and references therein). A TSM, which is a conceptual model, assumes that the stream system is comprised of a main channel connected to some well-mixed storage zones. The two key parameters of the model are an exchange coefficient and the extension of the storage zones. These parameters, which do not have a physical interpretation, need the tail of the breakthrough curve to be fitted. To this end, the data must necessarily cover the full duration of the tracer residence time, with a complete mass balance recovered in the river at the end, implying a long and unusually onerous experiment duration of up to a few days.

In order to improve the understanding of the surface water and groundwater exchanges, geophysical tools have been acknowledged to be very useful (McLachlan *et al.*, 2017), in particular the Electrical Resistivity Tomography (ERT) which can be used to track a salt tracer (Ward *et al.*, 2010, Ward *et al.*, 2012, Ward *et al.*, 2014) through the riverbed. In Ward *et al.* (2010) such a combination of ERT images with a salt tracer experiment allowed quantification of the cross-sectional area through which the tracer infiltrates into the HZ. Other tracer experiments were conducted by Ward et al. (2012, 2014) in a headwater mountain stream. One of the principle contributions of these studies is that four replicates of the same tracer experiment were performed during the same recession period. This led them to illustrate the inverse relationship between the HZ residence time and the river flux. The data treatment allowed quantifying the tracer arrival and residence time on the cross-section images. In all these publications, it seems that the river has not been explicitly taken into account as a limit during the data inversion, whereas Houzé et al (2017) have shown that imposing some known resistivity river values strongly influences the results, compared to a free inversion calculation.

Among the observations that have been made from in-situ tracer studies is the key fact that the HZ mixing is more pronounced when the river flow decreases. This has been observed both at the same location but under varying hydrodynamic behaviours over time (Harvey *et al.*, 1996, Ward *et al.*, 2012), and at various locations along the same river network, from the 5th order river to the headwater sites upstream (Ward *et al.*, 2019). This process, observed during these field studies, corresponds closely to the finding in theoretical studies associating more HZ mixing with less groundwater discharge flux. Indeed, the river recession or the catchment area decrease upstream from the river are certainly associated with a decreasing groundwater discharge rate, allowing more infiltration from the stream water into the HZ. The problem is that an exact estimation of the aquifer flux has never been achieved from this kind of field measurements.

The quantification of the groundwater discharge rate derived from field data is of significant interest in order to understand the HZ mixing processes at the field scale. As we will show, this objective can be followed combining physical models with field data. As noted by Cardenas (2015), “Very few studies have been able to compare model results with observations”. Furthermore, as recently mentioned by Lewandowski *et al.* (2019), “combining several types of studies at the same site and from multidisciplinary perspectives reduces the shortcoming of single methods, and thus, adds invaluable insight into processes in the HZ.” However, the literature on HZ highlights that it is difficult to associate numerical models with field measurements. Among the studies that combine experimental and modelling approaches within the HZ, three of them (Bouchez *et al.*, 2021, Cranswick *et al.*, 2014, Munz *et al.*, 2011) caught our attention because they used vertically distributed measurements within the HZ. Cranswick *et al.* (2014) used three environmental tracers, (temperature, radon and electrical conductivity), to characterize downwelling, neutral and upwelling hyporheic zones along a pool-riffle sequence in a natural river. Residence times derived from temperature and radon data showed considerable disparity which was attributed to the distinct influence of small-scale heterogeneity on temperature and radon transport. The numerical approach adopted in the paper had too many assumptions (1D geometry, constant parameters in space and time, diffusion and dispersion neglected) to succeed in simulating the residence time in the HZ. Munz *et al.* (2011) constructed a MODFLOW model based on hydraulic head measurements from nested multilevel piezometer network. As the investigated depth was deeper than the 15-30 cm superficial layer, they used the model to simulate the infiltration of the river water into the superficial

HZ. At a regional scale, Bouchez *et al.* (2021) showed that the estimation of groundwater-surface water exchanges by a numerical model could be improved in the case of gaining reaches by natural tracer data, sampled from multilevel vertical HZ profiles.

In this study, we drew inspiration from the abovementioned methodologies, combining HZ vertically-distributed field data and physics-based modelling in order to quantify the major parameters (e.g. the aquifer recharge flux and the sediment hydraulic conductivity) involved in HZ mixing processes. However, instead of measuring head, temperature or radon, we sampled the HZ water for chloride analysis, which allowed the monitoring of an artificial tracer test with a NaCl solution injected into the river and tracked within the HZ. In order to get a better idea of the spatial behaviour, we added ERT images of the HZ, before and during the artificial test experiment. The chosen model was the HydroGeoSphere code (Therrien *et al.*, 2012), coupling the surface water and groundwater flows, which is rarely used to study the HZ mixing processes. Various numerical scenarios were considered in order to analyse the respective influences of the various parameters on the mixing zone extension.

## 2-Material and methods

### *2.1 Study area*

Experiments were performed at the Ambart island site on the Essonne River, a tributary of the Seine River, about 50 km south of Paris (Fig. 1). The Essonne catchment (1840 km²) is made up of sedimentary formations of the Parisian Basin (Vernoux, 2001). The main aquifer here lies within the Eocene layers with mainly calcareous and sandy lithologies; it is rather productive and flows towards the river (Vernoux, 2001). The mean Essonne slope is $10^{-4}$-$10^{-3}$ (Houzé, 2017). At the site of Ambart Island, the eight-meter-wide right arm of the river was artificially filled with rock fragments and pebbles for 20 meters, resulting in a 50-centimeterhigh step in the river bottom, with a 2.5-meter-long inclined plane between the two horizontal planes (Fig. 1).

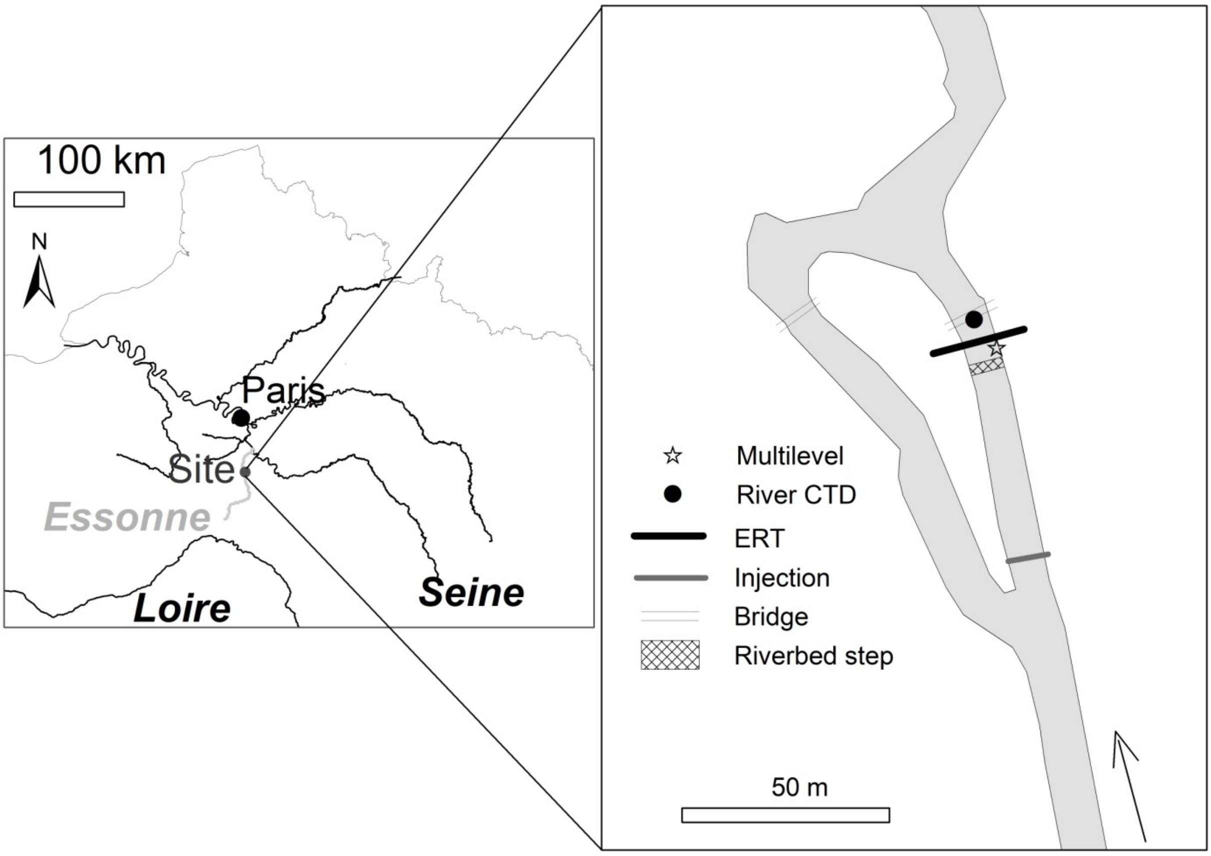

Figure 1. Location of the study area and important objects for the experiment

## *2.2 Experiment description*

In order to trace the river water through the HZ, a salt solution was injected into the river for one hour. This salted solution was prepared before the experiment from the dissolution of 100 kg of solid NaCl in 500 l of river water, leading to a conductivity value of 222 $mS.cm^{-1}$. The injection system was installed at the beginning of the right river arm, 51 m upstream from the HZ sampling point (Fig. 1). In order to evenly distribute the salt solution in the river, sprinklers were suspended above the river and connected to the 500 l tank by an electric pump. The total duration of the injection was one hour (between 12:30 and 1:30pm). Measurements were made before, during, and until four hours after injection. Both geochemical and geophysical measurements were performed to trace the salt solution through the HZ:

- a device continuously measured the pressure and the conductivity in the river,
- pore water samples were collected from the riverbed sediments at regular intervals for chloride analyses,
- Electrical Resistivity Tomography (ERT) was performed along the river cross section (Fig. 1).

Figure 2 summarizes the chronology of the various measurement steps, with 8 sample sets, and 7 ERT images.

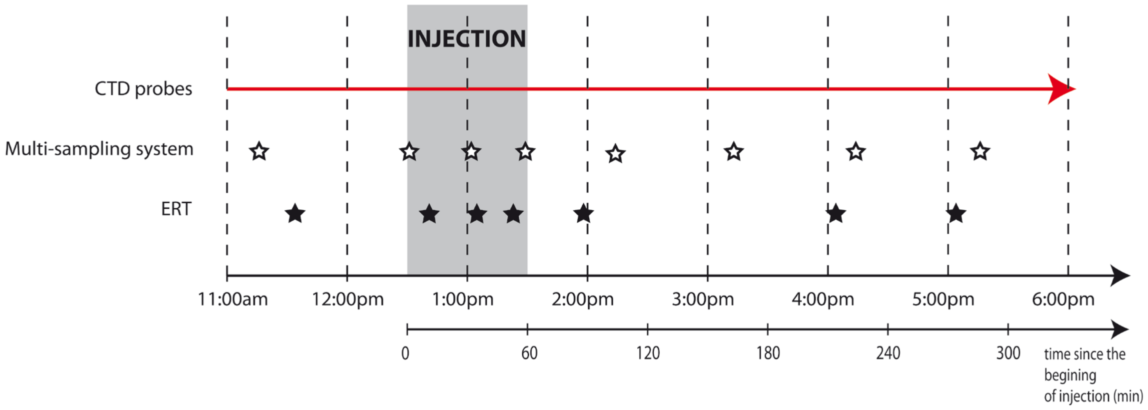

Figure 2. Chronology of all the measurements during the experiment

The river discharge was measured with the help of a mechanical current meter from SEBA Hydrometrie before and after the experiment. A calibration curve linking the quantity of salt dissolved into the water to the measured conductivity was done in the laboratory: it was performed with some water from the river and with some of the same salt as that used for the tracer experiment. This calibration was used to estimate the quantity of chloride recovered at the CTD monitoring section. The experimental methods are described below.

### *2.3 Tracer measurement*

A Conductivity Temperature Depth (CTD)-Diver (Schlumberger model, precision $10^{-3}$ mS.cm$^{-1}$ for the conductivity and $10^{-3}$ cm for the water level) was placed in the middle of the river to measure the in-stream electric conductivity. It was protected by screened PVC tubes and located just downstream from the studied area (see location in Fig. 1). To get more details on the riverbed water composition, a multilevel sampling device (Rivett *et al.*, 2008) was inserted 130 cm deep into the riverbed sediments, at 1.5 m from the river bank (Fig. 1). This device allowed sampling pore water from 6 cm to 124 cm deep, through a series of 11 capillar 1 mm internal diameter Teflon tubes that were fixed approximately every 10 cm around a 1.8 cm external diameter PVC tube. The length of the Teflon tubes was extended to 4 m in order to perform the water sampling from the riverbank and consequently to avoid any human presence in the river during experiment. The sampling was done with manual syringes, simultaneously pumped and blocked with sticks, as it could take up to 10 min to pump a reasonable volume of pore water (10 ml max plus 5 ml of dead volume). The samples were directly filtrated through a 0.45 µm membrane, and stored in hermetically sealed glass bottles. Chloride analyses were performed in the laboratory with a Dionex ICS 1000 chromatography device, using an ion pack AS 14 column and ion guard AG 14 pre-column, an AERS 500 self-regenerating suppressor and a suppressed conductivity detection. The eluent was a mix of 3,5mM sodium carbonate and 1.0 mM sodium bicarbonate, with a flow rate of 1.2 mL.min$^{-1}$ for a 15 minute long complete analysis.

### *2.4 Electrical resistivity tomography*

A line with 48 electrodes was installed across the 8-meter wide river and the banks. It was located 2.5 m downstream from the multi-sampling system (Fig. 1). The total length of the ERT line was 23.5 m with an interval between electrodes equal to 50 cm. The electrodes installed within the river were isolated at the top with insulating tape to ensure the electrical contact only with the riverbed sediments. In order to avoid current loss into the water column, the connecting cables were suspended above the river.

The data acquisition was done with a 48 multi-electrodes Syscal Pro device (Iris Instruments) that was connected to the electrode line. The chosen configuration for acquisition was the dipole-dipole with the multiplex option leading up to 10 simultaneous measurements. The fast mode was used in order to spare the acquisition duration: the minimum acquisition duration was 10 min. After having reported the precise topography of the location of each electrode, as well as the local water depth and the river-varying resistivity value where necessary, the data inversion took into account the real topography and the known water thickness above each electrode located within the river.

The commercial software Geotomo Res2Dinv (Loke and Barker, 1996) and the so-called robust inversion method were used to interpret the data. The minimisation of a mixed L1-norm was undertaken as an iteratively re-weighted least-squares algorithm. This minimisation is more suitable when the subsurface has sharp boundaries and we have found that such models better represent the geological reality of the studied site. The image obtained before the injection (Fig. 3) shows distinct layers underneath the river: a thin layer just below the stream, with high resistivities (>300 Ohm.m), and a thicker zone that is also more conductive (resistivity < 100 Ohm.m). These two layers can be interpreted respectively as a sandy and permeable zone assumed as backfill associated to the bridge construction and a clayey less permeable zone. The first layer thickness was estimated around 25 cm.

As for the images done during and after the injection, the time-lapse mode of the Res2Dinv software was used and different constraints are available to perform the inversion process. We chose the "no constraints" option, which subsequently determines the resistivity changes by comparing the model resistivity values obtained by inversion with an initial data set and the later time data set. With this option, theoretically there is no guarantee that the observed changes are only due to variations in resistivity with time (changes in electrode contact, modelling artefacts). However, the relatively short duration of the experiment (a few hours) allows us to assume the acquisition was done exactly in the same conditions. Other constraints have also been tried out and the results are quite similar in all cases. Therefore, we chose to not add constraints for the inversion process.

As there are large resistivity contrasts in the ERT section (see Fig. 3) we have chosen a sequential inversion, which means that the inversions of the later time steps only start after the inversion of the initial model. We used this initial model as the reference model for all the subsequent time data sets. As a rule, we have chosen not to overly constrain the inversion process and this provides acceptable models even if it is not a full time-lapse inversion.

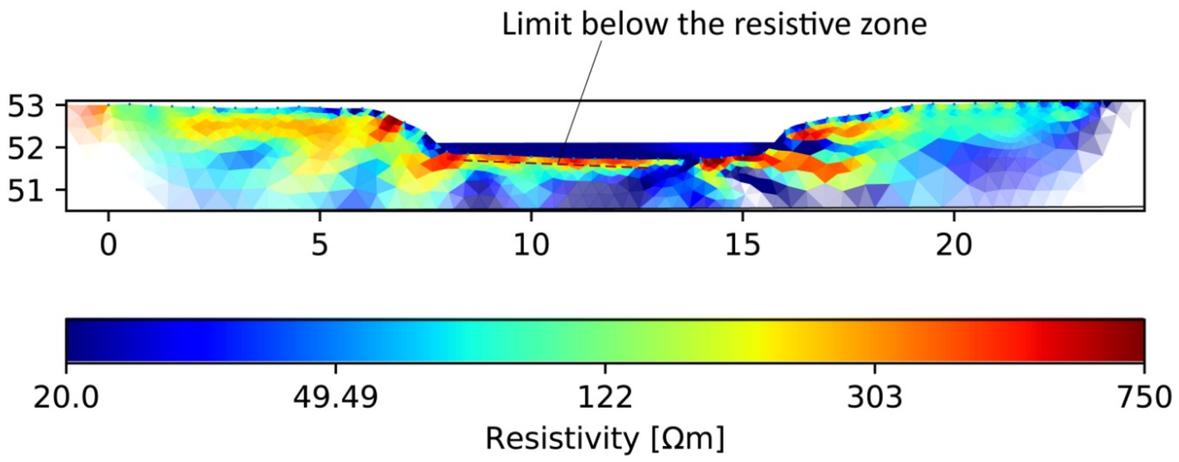

Figure 3. Reference ERT profile from West to East, before the injection; the distances are given in meters. The river is represented with the resistivity values that were taken into account as a constraint.

### *2.5 Modelling*

Field experiments were combined with a modelling approach performed with the HydroGeoSphere (HGS) code (Therrien *et al.*, 2012). HGS models the coupling between surface and subsurface flows. It also models the transport of non-reactive tracers. HGS is particularly well suited to model river-groundwater interactions (Brunner *et al.*, 2017). The appendix gives a brief overview of the equations used to simulate the surface and subsurface flows and the transport in HGS. A full description of the physical processes, the equations, and the numerical schemes can be found in Therrien *et al.* (2012).

The aim of this modelling was not to construct a precise model of the Ambart island site but rather to use a simplified model of the site in order to identify the main factors that drive the tracer transport within the HZ. As a consequence, we did not perform 3D simulations that would have implied very long computing times and a lot of unavailable data (e.g., Digital Elevation Model, hydraulic conductivity and diffusivity heterogeneities). Instead, calculations were performed on a pseudo 2D vertical domain that modelled a 51 m long, 8 m wide, and 2 m deep longitudinal transect of the river (Fig. 4). The top of the domain, which represents the topography of the riverbed, was designed according to a longitudinal profile measured at the middle of the river. It was characterized by a downstream 2.5 m long and 50 cm high step and a mean slope of $10^{-3}$ on both sides of the step (Fig. 4). The domain was made of two superposed layers, from the ERT interpretation, with assumed homogeneous hydraulic conductivities. During the calibration process, the first layer thickness was found to be 26 cm, very close to the value, 25 cm, that was estimated from the reference ERT profile. The pseudo 2D domain was discretized into 118 columns, 2 rows and 100 layers of elements. The spatial resolution along the slope was equal to 1 m except around the measurement area where it was refined to 0.25 m. The vertical resolution was finer at the top of the subsurface domain (1 cm) and coarsened towards the bottom (from 2 cm to 5 cm). The spatial resolution along the third direction was equal to 4 m. This third direction was only added in order to apply the surface boundary conditions and for the data post-processing. The adaptive time stepping was provided in the simulation with time-step incrementing and decrementing factor limits of 2 and 0.5, respectively. A constant water depth of 1 m as a boundary condition and a critical depth boundary condition were applied at the river inlet and outlet, respectively. To avoid any influence of the critical depth boundary condition on the numerical results, the total length of the domain was extended to 1000 m downstream. Only the numerical results in the upstream 51 m of the domain will be discussed in the following sections. A flow boundary condition was applied at the bottom side of the subsurface domain for modelling the upward flux from the groundwater to the river. This flow boundary condition was assumed constant because the simulated experiment lasted only a few hours. The subsurface domain was initially water saturated and the water depth at the surface was initially equal to 50 cm above the observation zone. The initial chloride concentration $[Cl^{-}]_0$ was equal to 29.4 $mg.l^{-1}$ in the whole domain. A constant chloride concentration $[Cl^{-}]_{GW}$ equal to 17.7 mg/l was applied at the bottom of the domain. These two values were chosen because they correspond to the chloride concentrations before the tracer experiment in the river and in the groundwater, respectively. A first calculation with a constant $[Cl^{-}]$ applied at the river inlet ($[Cl^{-}]$ = 29.4 $mg.l^{-1}$) was performed in order to obtain a steady state for the flow and for the chloride concentration. The resulting steady state was then used as an initial condition for the simulation of the tracer experiment. In the experiment, a total volume of water equal to 500 l was injected into the river during one hour. This quantity is negligible compared to the river discharge that was approximately equal to 0.17 $m^3.s^{-1}$. As a consequence, we assumed that 100 $kg.h^{-1}$ of NaCl were injected into the river during one hour, i.e. 60.66 $kg.h^{-1}$ of chloride. As the river discharge was ~0.17 $m^3.s^{-1}$, the corresponding chloride concentration was equal to 99.1 $mg.l^{-1}$. Finally, the total concentration $[Cl^-]_{inj}$ was equal to the sum of this concentration and the natural chloride concentration of the river. We obtained $[Cl^-]_{inj}$ = 129 $mg.l^{-1}$. This chloride concentration was imposed over the course of one hour at the upstream boundary of the surface domain.

The Manning roughness coefficient, which represents hydraulic resistance to flow, is often determined empirically. It was manually calibrated with the experimental profiles measured during the tracer injection (from t=0 to t=60 min) in order to correctly simulate the velocity of the surface flow and the resulting tracer transport. We obtained $n$=0.1 s $m^{-1/3}$. This value is in the range of values that are usually used (0.01 < $n$ < 0.5 (Woolhiser, 1975)). We imposed a free-solution diffusion coefficient equal to $2\times10^{-9}$ $m^2.s^{-1}$ (Freeze and Cherry, 1979). The longitudinal dispersivity $\alpha_{lo}$ of the surface flow domain was assumed to be equal to 5 m. The longitudinal dispersivity $\alpha_l$ of the subsurface domain at the experiment scale was estimated with the empirical power law of Schulze-Makuch (2005):

$$D_l = \mathrm{c} \times \mathrm{L}^{0.5} \quad (1)$$

where L is the flow distance, and c is a parameter characteristic of the geological medium, which varies between c~0.01 m for sandstones and unconsolidated media, and c~0.8 m for carbonate rocks. With c=0.01 and a flow distance L equal to 51 m, we obtained $\alpha_l$ ~ 0.1 m, and took a transverse dispersion coefficient $\alpha_t$ equal to $\alpha_l$ /10. The values of the saturated hydraulic conductivities of the top and bottom layers, $K_1$ and $K_2$, and the value of the groundwater flux imposed at the bottom of the domain, $F_0$, were manually calibrated with the chloride concentration profile measured in the sediments before the tracer experiment. Table 1 provides the input parameters used for the simulation and specifies which parameters were measured, estimated or calibrated. Only manual calibrations were performed.

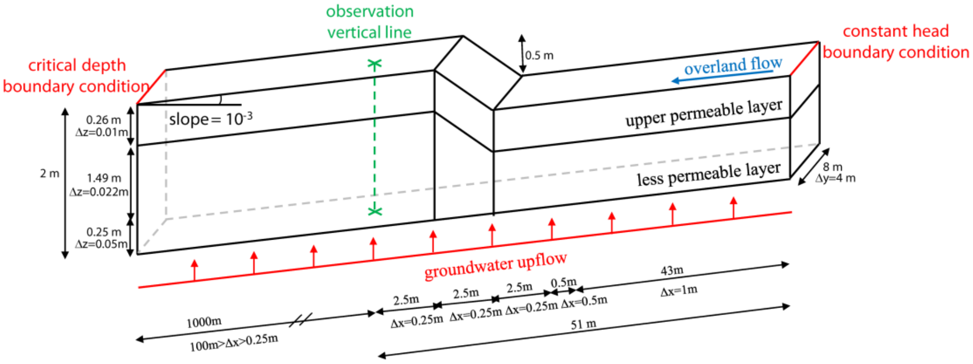

Figure 4: Geometry and boundary conditions of the pseudo 2D model setup

Table 1: Surface and subsurface parameters and conditions for the numerical simulation of the tracer experiment.

| Parameter | Symbol | Value | Units | Notes |
|---|---|---|---|---|
| <u>*Surface*</u> | | | | |
| *Flow and transport properties* | | | | |
| Manning roughness coefficient | $n$ | 0.1 | $s.m^{-1/3}$ | Calibrated[a] |
| Longitudinal dispersivity | $\alpha_{lo}$ | 5 | m | Assumed[b] |
| Molecular diffusion coefficient | $D_{free}$ | $2\times10^{-9}$ | $m^2.s^{-1}$ | Literature value[c] |
| *Flow boundary conditions* | | | | |
| Water depth at the river inlet | | 1 | m | Measured |
| Critical depth at the river outlet | | | | |
| *Tracer conditions* | | | | |
| Initial chloride concentration | $[Cl^-]_0$ | 29.4 | $mg.l^{-1}$ | Measured |
| Injection chloride concentration | $[Cl^-]_{inj}$ | 129 | $mg.l^{-1}$ | Estimated[d] |
| Injection duration | T | 3600 | s | Experimental condition |
| <u>*Subsurface*</u> | | | | |
| *Flow and transport properties* | | | | |
| Upper layer thickness | | 0.26 | m | Calibrated[e,f] |
| Upper layer saturated hydraulic conductivity | $K_1$ | $5\times10^{-2}$ | $m.s^{-1}$ | Calibrated[f] |
| Lower layer saturated hydraulic conductivity | $K_2$ | $1\times10^{-3}$ | $m.s^{-1}$ | Calibrated[f] |
| Upper layer porosity | $\theta_{s1}$ | 0.9 | - | Measured |
| Lower layer porosity | $\theta_{s2}$ | 0.5 | - | Measured |
| Subsurface longitudinal dispersivity | $\alpha_l$ | 0.1 | m | Estimated[g] |
| Subsurface transverse dispersivity | $\alpha_t$ | 0.01 | m | Assumed equal to $\alpha_l/10$ |
| Tortuosity | $\tau$ | 1 | - | Assumed |
| Molecular diffusion coefficient | $D_{free}$ | $2\times10^{-9}$ | $m^2.s^{-1}$ | Literature value[c] |
| *Flow and transport boundary conditions* | | | | |
| Groundwater flux imposed at the bottom | $F_0$ | $4\times10^{-6}$ | $m.s^{-1}$ | Calibrated[f] |
| Chloride concentration at the bottom | $[Cl^-]_{GW}$ | 17.7 | $mg.l^{-1}$ | Estimated[d] |

[a] Manual calibration with the velocity of the surface flow and the vertical profiles of the chloride concentration.

[b] Three other simulations performed with $\alpha_{lo}$= 0.5, 5, and 50 m showed that the vertical profiles of the chloride concentration were not sensitive to $\alpha_{lo}$

[c] Freeze and Cherry (1979) p. 103

[d] Estimated from field observations or from experimental conditions

[e] Estimated from the ERT profile before the tracer experiment

[f] Manual calibration to match the vertical profile of the chloride concentration measured before the tracer experiment

[g] Estimated from the literature (Schulze-Makuch, 2005): $\alpha_l$~0.01×L with L=51 m

A modelling approach is very useful for analyzing the respective influences of various parameters on the mixing processes. First, we performed two other simulations for testing the effect of the upper layer hydraulic conductivity, with values equal to $0.2 \times K_1$ and $5 \times K_1$, respectively. Secondly, we studied the sensitivity of the mixing zone extension to ambient groundwater flow conditions represented by changes in groundwater flux. Three scenarios were considered: (1) a gaining river (the groundwater flux, denoted F, which is imposed at the bottom boundary of the model domain, is positive); (2) a neutral scenario (F=0); and (3) a losing river (F<0).

## 3-Results

### *3.1 Tracer data*

Figure 5 displays the temporal evolution of the water conductivity in the river that was monitored by the CTD probe during the tracer experiment. Two peaks of conductivity are clearly visible. They are due to a variation of the salt injection flow rate during the first 20 minutes of the experiment. Before the injection, the conductivity of the river was about 600 µS $cm^{-1}$. During the injection, the conductivity of the river water increased to 900 µS $cm^{-1}$. After the injection, the conductivity sharply dropped back to its initial value. The river flow rate before and after the experiment was equal to 0.17 $m^3.s^{-1}$ and 0.22 $m^3.s^{-1}$, respectively, with an estimated error of 10 %.

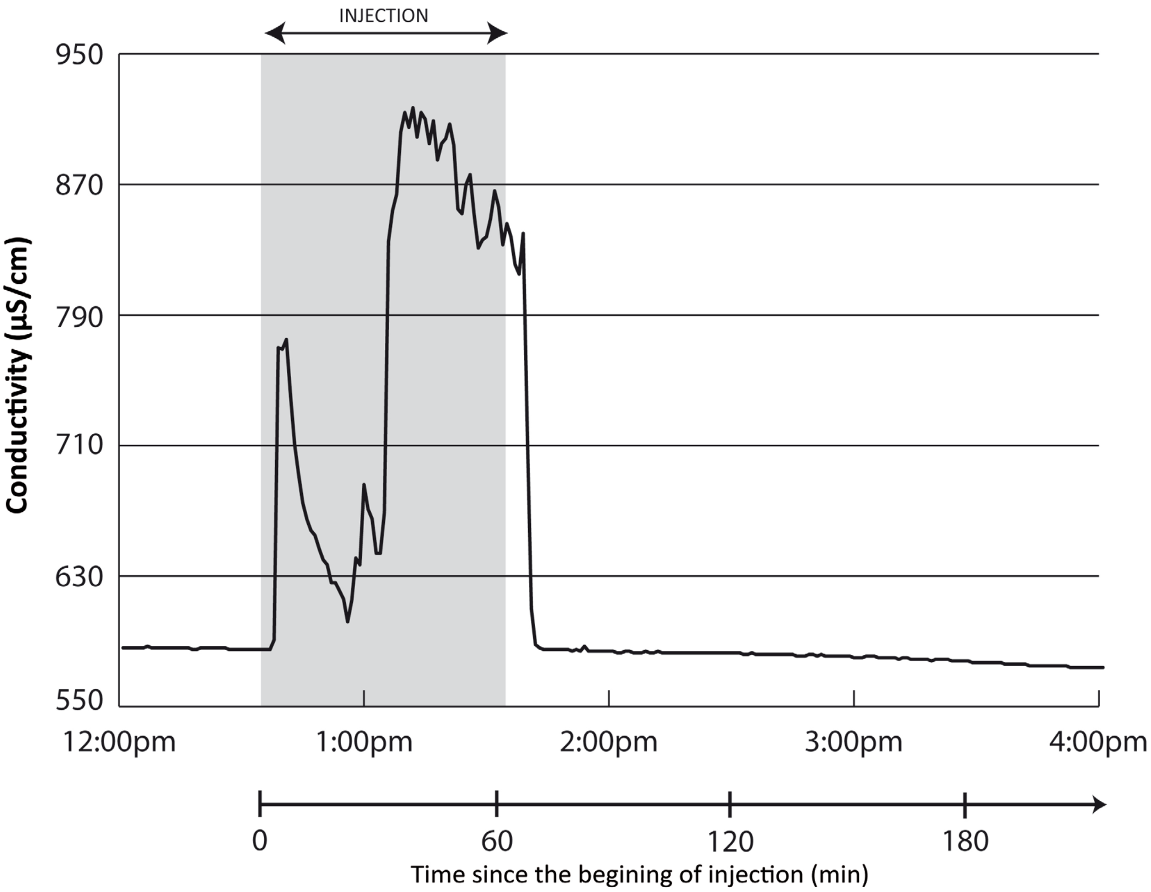

Figure 5. Evolution of the water conductivity in the river before, during, and after injection of a salt solution in the river

Figure 6 displays the results of the chloride analysis in the multi-sampling system (see location of the multi-sampling system in Fig. 1), at eight various times. Each complete sampling set lasted between 10 and 15 minutes. The initial time t=0 in Fig. 6 corresponds to the beginning of the injection experiment (t=12:30 pm in Fig. 2). The value at 0 cm depth corresponds to the chloride concentration measured in the river water. A reference profile was achieved before the beginning of the injection (red line in Fig. 6). The chloride concentration in the river before injection was equal to 29.4 mg.l$^{-1}$. As can be seen in Fig. 6, before injection, the chloride concentration decreased from 29.4 mg.l$^{-1}$ to 17.7 mg.l$^{-1}$ through the first 40 cm within the sediment. From the distinct chloride values measured in the river and along this reference profile, the depth of the HZ can be estimated at 35 cm if we consider a threshold of at least 10% of surface water within the sediments to define the HZ (Triska *et al.*, 1989).

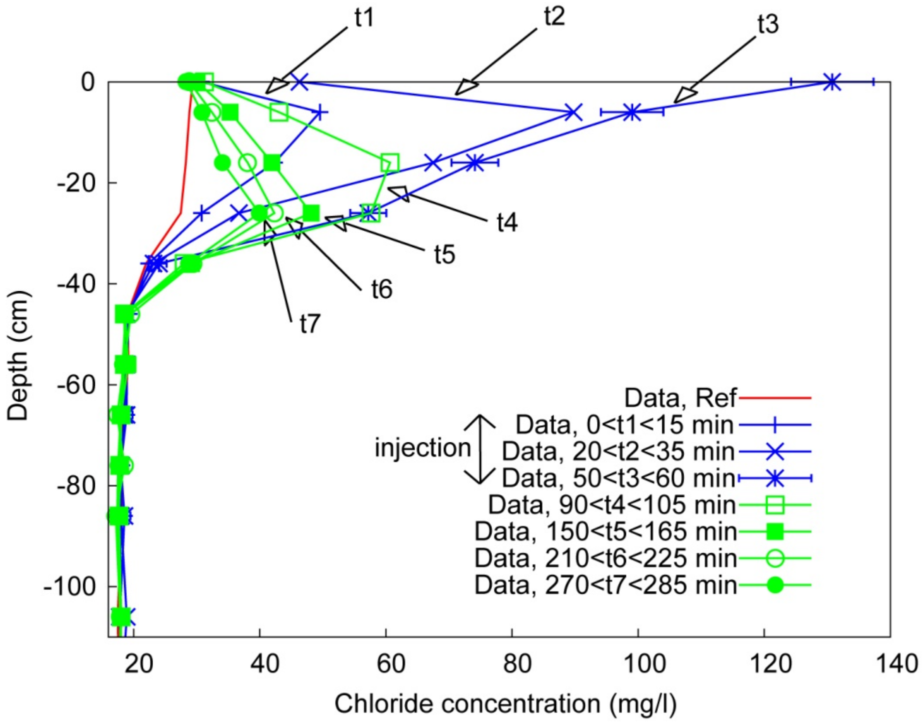

Figure 6. Experimental vertical profiles of the chloride concentration in the pore water measured with the multi-sampling system before, during, and after injection. Error bars are equal to 5%. For clarity, they have only been added to one of the profiles.

The profiles made during and after the injection show a rapid change in the chloride concentration within the riverbed sediments. The three profiles from t = 0 to t = 60 min were achieved during the injection (blue curves in Fig. 6). The chloride concentration in the first 35 cm-deep sediments clearly increased during the injection until values much higher ($\geq 100$ mg.l$^{-1}$) than the initial ones ($\leq 30$ mg.l$^{-1}$) were observed. With the exception of the profile for $50 \leq t \leq 60$ min, the concentrations measured in the river were always lower than those measured in the superficial sediments. The sampling system in the river, using Teflon extensions, only allowed very local sampling. Therefore, the measured values were certainly not representative of the maximum concentration in the river, especially if the mixing was not perfectly homogeneous within the river. The highest value measured in the river at $50 \leq t \leq 60$ min reached 130 mg $l^{-1}$ (profile “t3” in Fig. 6). Concentration in the sediments at a given depth increased with time during the injection period. After the end of injection, concentrations in the river quickly dropped to the initial concentration of ~ 30 mg.$l^{-1}$. By contrast, the chloride concentration remained higher in the sediments than its initial value until the end of the monitoring. The peak of concentration progressively infiltrated into the sediment down to 35 cm deep. Beyond this limit, no significant variation of the chloride concentration was observed.

### *3.2 ERT*

Figure 7 displays the ERT time-lapse profiles obtained during and after the tracer injection, expressed as the percentage difference from the reference profile to highlight the variations due to the injection of salt into the river. Some zones showing a decreased resistivity (≤ - 40 %) appeared below the riverbed and under the banks during the injection.

Under the banks, the initial resistivity values (cf Fig. 3) were very heterogeneous, due to the artificial material used during the bridge construction: some more resistive zones with tongue shapes could be interpreted as sandy zones which could easily conduct the tracer through the banks. A quick tracer infiltration could indeed lead to the decreased resistivity zones observed under the banks in Figure 7. However, as Figure 7 also shows increased resistivity zones under the banks, one could conclude that the decreased resistivity zones might be due to some inversion artifacts, compensating for the increased resistivity zones.

These potential artifacts were only observed under the banks and limited our capacity to interpret the data.

Below the riverbed, the decreased resistivity zones showed multilayered behaviour: a subsurface layer (about 0-25 cm depth), distributed across the whole riverbed width, showed resistivity variations of 20-30 % during the injection (from 35 to 52 min), and recovered its initial values after the injection (at 87 min). The underlying layer (about 25-80 cm depth) showed the strongest resistivity variations (decrease of more than 40 %). The behavior of this layer seemed homogeneous during the tracer injection, but demonstrated heterogeneity during the tracer retrieval, with remaining lower resistivity zones between 7-8 m across the profile (Fig. 7) and from 9-12 m across the profile. In the deeper layer (> 80 cm depth), the tracer infiltration was heterogeneous across the profile: at the beginning, the impacted zone was located between 9 and 10 m across the profile, but at 52 min the lower resistivity zone appeared at 10-12 m across. The decreased resistivity values remained after the injection within both zones alternately. One has to note that the initial resistivity values in this deep layer (cf Fig. 3) were very low (about 20 Ohm.m), implying that only small quantities of tracer were necessary to show a resistivity variation. Moreover, the resolution in deep zones is weaker than in the subsurface zones, associated with the ERT method. It is assumed here that the first ~ 25 cm layer is more permeable than underneath, as the tracer is quickly removed from this layer. Concerning the other observations, their complexity and potential associated artifacts make their interpretation weak.

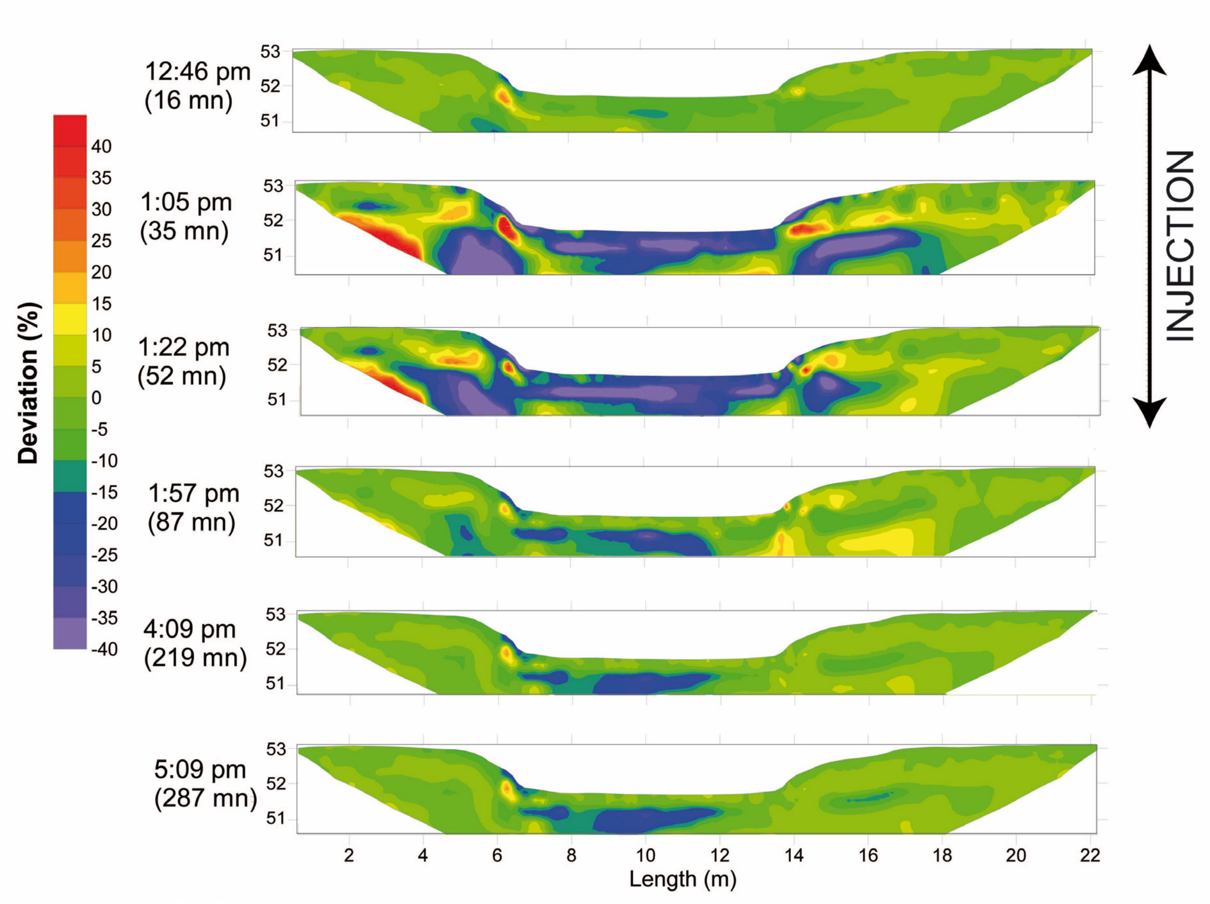

Figure 7. Monitoring of ERT images expressed as percentage change in resistivity compared to the reference profile that was recorded before the beginning of the injection

## *3.3 Modelling*

### *3.3.1 Manual calibration*

The 2D configuration presented in Section 2.5 and in Fig. 4 was used to simulate the salt transport during and after the injection experiment. As a first step, the values of the saturated hydraulic conductivities in the top and bottom layers, $K_1$ and $K_2$, and the value of the groundwater flux imposed at the bottom of the domain, $F_0$, were manually calibrated with the chloride concentration profile measured in the sediments before the tracer experiment (profile "Ref" in Fig. 6). We obtained $K_1 = 5 \times 10^{-2}$ m.s$^{-1}$ and $F_0 = 4 \times 10^{-6}$ m.s$^{-1}$. Figure 8 shows the calibration results, testing other values of $K_1$ (factor 5 applied) and $F_0$ (factor 10 applied). Tests for lower or higher values of $K_1$ show respectively a lower or higher slope in the upper part of the vertical profile of the chloride concentration (Fig. 8a). This is associated with the increasing capacity of this upper layer to allow river water to infiltrate, with a higher slope showing a greater proportion of river water. Figure 8b shows that increasing $F_0$ results in a decrease in mixing thickness. It is due to the increasing pressure exerted by the aquifer discharge, limiting the river infiltration towards the bottom of the domain. These tests show that the initial vertical profile of chloride allowed us to fit $K_1$ and $F_0$ (the coefficient of determination $R^2$ is equal to 0.99). The results were not sensitive to the saturated hydraulic conductivity of the deeper layer, $K_2$, as long as $K_2$ was low enough ($K_2 \leq K_1 / 10$). We took $K_2 = 10^{-3}$ m.s$^{-1}$.

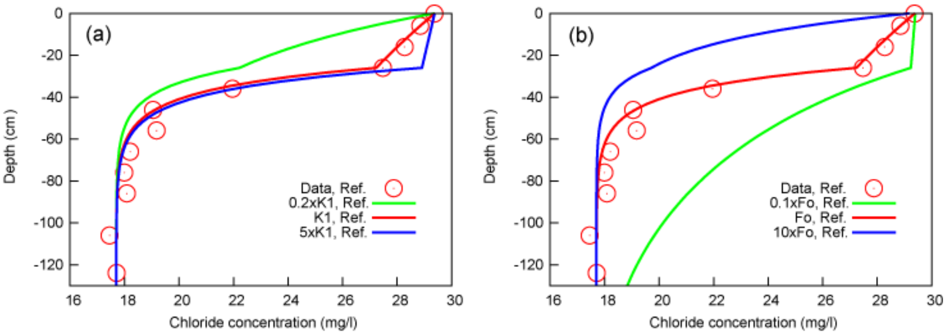

Figure 8. Vertical profiles of the chloride concentration in the pore water before the tracer experiment. In each figure, symbols indicate measured data while the solid lines indicate modelled results obtained (a) with distinct values of the upper layer hydraulic conductivity, and (b) distinct values of the groundwater flux imposed at the bottom of the model domain

### *3.3.2 Tracer experiment simulation*

Figure 9 displays the vertical profiles of chloride concentration obtained from the modelling approach after calibration. Symbols correspond to the measured profiles already given in Fig. 6. As can be seen, the simulated profiles corresponded closely to the experimental ones. During injection into the surface flow, the tracer entered deeper into the sediment. After injection, some of the tracer still remained in the sediment at a depth of 40 cm, even after several hours.

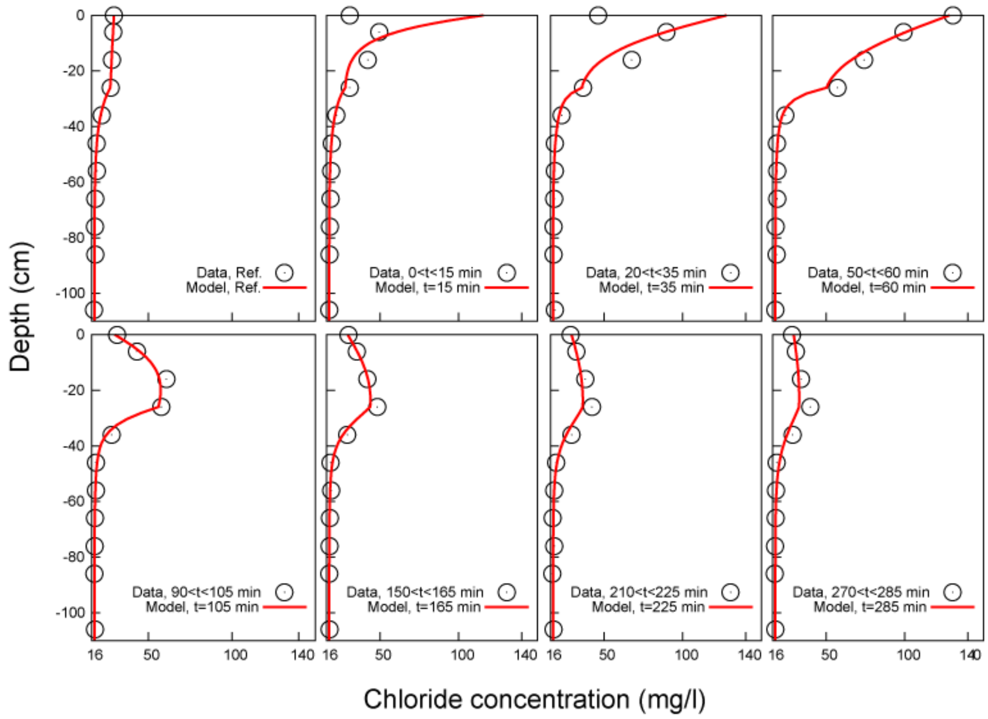

Figure 9. Simulated vertical profiles of the chloride concentration in the pore water obtained with the 2D model at the same place and at the same times as the observed values. In each figure, symbols indicate measured data while the solid lines indicate modelled results.

### 3.3.3 Other scenarios

The effect of the groundwater flux on the mixing zone extension was investigated using three types of numerical scenarios: (1) gaining (the groundwater flux, denoted F, which is imposed at the bottom boundary of the model domain, is positive); (2) neutral (F=0); and (3) losing (F<0). Figure 10 displays the snapshots of the simulated chloride concentration fields under three gaining scenarios ($F = 10 \times F_0$, $F = F_0$, and $F = 0.1 \times F_0$, where $F_0 = 4 \times 10^{-6}$ m.s$^{-1}$ corresponds to the groundwater flux previously used for simulating the field experiments). Figure 10 also shows the results of the neutral scenario, and two losing scenarios ($F = -1 \times F_0$, and $F = -10 \times F_0$). A 10-meter long zone around the downstream step is shown. Results at t=0 correspond to the steady-state concentrations and flow directions before injection (first line in Fig. 10). The other snapshots show the simulated chloride concentration fields at t = 35, 60, 105, 225 and 285 min after the start of the injection, respectively. These times correspond to some of the sampling times. The last snapshot is given 30 h after the injection, as a prediction scenario.

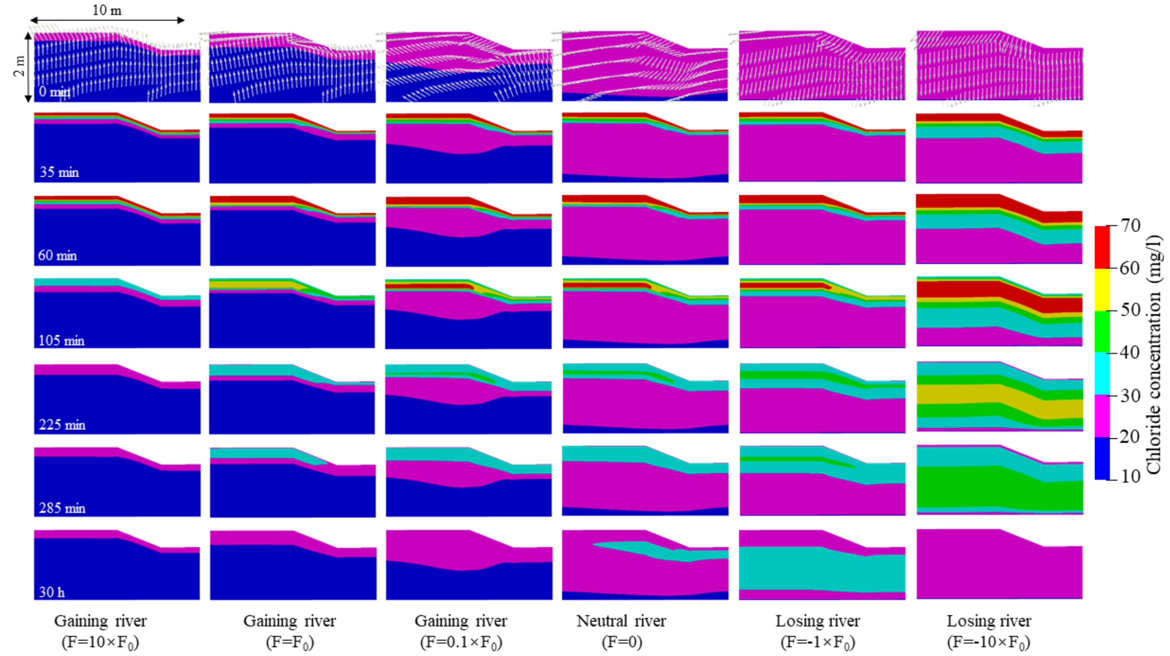

Figure 10. Time evolution of the simulated chloride-transport fields under three different river conditions: gaining, neutral, and losing river. The three different conditions are imposed by changing the groundwater flux at the bottom boundary of the model domain. Steady-state flow directions are indicated at t=0 (arrows are of equal lengths and do not indicate magnitude).

These simulations allowed us to quantify the relative mass change associated with the tracer infiltrated into the HZ. Figure 11 shows the time evolution of the relative mass change of chloride in the HZ, i.e. the ratio (Total mass at each time-step – Initial total mass) / Initial total mass, for the three distinct river conditions: $F = 10 \times F_0$, $F = F_0$, and $F = -10 \times F_0$. Each curve showed a peak whose intensity depends on the type of scenario. The maximum value (0.54) was obtained for the losing river condition. For the gaining river conditions ($F > 0$), the higher the F value, the lower the peak intensity (from 0.35 to 0.24). This highlights the fact that when aquifer discharge decreases, more river water infiltrates into the HZ.

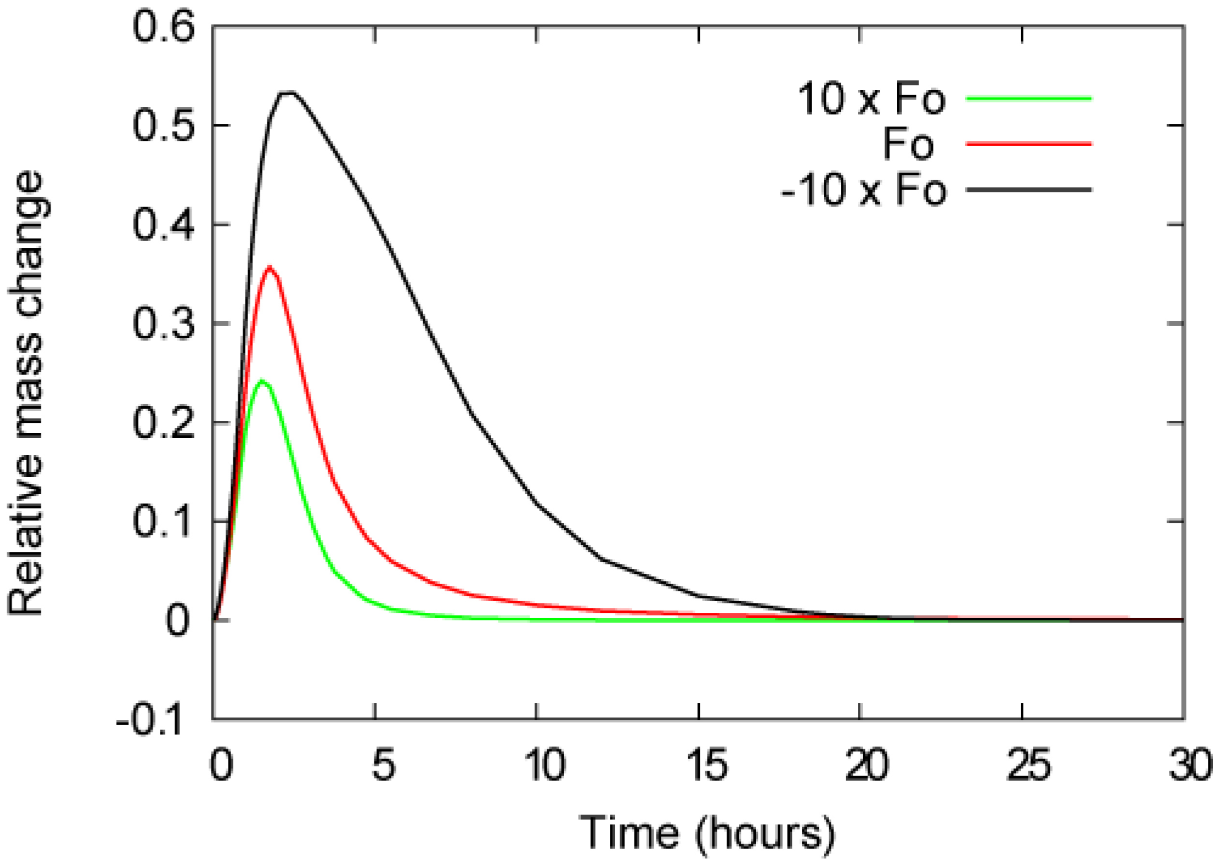

Figure 11. Time evolutions of the relative mass change of chloride in the HZ for the three distinct river conditions: $F=10\times F_0$, $F=F_0$, and $F=-10\times F_0$

## 4. Discussion

The approach developed in this study combines both experimental and modelling tools. As this combination is complex and quite rare, simplifications to the protocol were implemented. In this section, in order to underline the main insights of the study, we discuss certain parameters' influence on river water infiltration through the HZ as well as the advantages and disadvantages of the chosen protocol.

### *4.1. Impacts of the saturated hydraulic conductivity and the groundwater discharge flux*

The purpose of the manual calibration presented in Section 3.3.1 was not to obtain a precise value of the model parameters, but rather to determine the processes that drive the transport of salt into the HZ. Results showed a marked sensitivity of the chloride vertical profile to the upper layer saturated hydraulic conductivity and to the groundwater flux. These two parameters are the main drivers of the shape of the chloride profile within the hyporheic zone. This result is in agreement with theoretical studies (Boano et al., 2009, Cardenas and Wilson, 2006, Fox et al., 2014, Su et al., 2020).

As the difference between the chloride concentration of the river water and the groundwater was large, the chloride fields were very sensitive to the value of the groundwater flux (see Fig. 10). The stronger upward groundwater flow in the gaining river condition, the thinner the area of the mixing zone. It was also noted that the only case for which the step had any influence on the mixing zone behind it was when the aquifer discharge flux was around $4 \times 10^{-7}$ m.s$^{-1}$ (third column in Fig. 10), i.e. a non-zero but low enough value to allow the morphology to have an impact on the mixing. Otherwise, the mixing here was mainly allowed by the highly saturated hydraulic conductivity of the first riverbed layer, and inhibited at depth by both the effects of the lithology contrast and the groundwater pressure. On the other hand, the stronger downward groundwater flow in the losing river condition, the thicker the mixing area. The chloride field is therefore a good indicator of river conditions. As the hydraulic conditions were not modified during the injection of chloride in the river, the mixing area that could be traced by chloride for each given river condition did not change. During and after injection, the peak of chloride concentration was higher and deeper under the losing river condition.

From Figure 11, which shows the time evolution of the relative mass change of chloride in the HZ, it is possible to quantify the respective residence times corresponding to each F value. Taking a relative mass change of 0.01 led to estimated residence times of 5.7 h, 11.8 h and 17.8 h for aquifer discharge fluxes of respectively $10 \times F_0$, $F_0$ and $-10 \times F_0$. It shows exponentially decreasing behaviour, with decreasing residence time when the aquifer discharge flux increased. This is consistent with the results found, for instance, in Hester and Doyle (2008).

### *4.2. Advantages and limitations of the chosen protocol*

Compared with purely theoretical studies, the novelty of the paper lies in the combination of experimental and modelling approaches. Here, a multi-process model was constrained by the experimental vertical chloride profiles obtained within the HZ at distinct times, and led to an examination of the respective influences of the main factors controlling mixing between the river and the aquifer. By combining field experiments and modelling, our results confirmed conclusions already drawn by some authors from only numerical simulations or laboratory experiments (Boano *et al.*, 2009, Cardenas and Wilson, 2006, Fox *et al.*, 2014, Hester and Doyle, 2008, Su *et al.*, 2020): the most important factors controlling hyporheic exchange are the sediment hydraulic conductivity and the groundwater discharge rate towards the stream.

Before exploring the experimental results, we reflect on prior studies that combined field data and modelling. In Bouchez *et al.* (2021), the estimation of the regional aquifer discharge flow towards the HZ could be derived from numerical simulation and natural field tracer measurements, but no quantification of the river water infiltration through the HZ was done, as it was not the purpose of this specific regional study. In Munz *et al.* (2011), the surface water infiltrating through the HZ was simulated, but could not be validated by field data, as these did not investigate the corresponding 15-30 cm superficial layer. In Cranswick *et al.* (2014), the residence time within the HZ was derived from simulations varying temperature and radon measurements, but the authors acknowledged that their model was too simplistic to reproduce the potential vertical heterogeneities in the hydraulic conductivities, which handicapped the validation of this quantification, which is very different between the two types of measurements.

In this study, the values of both the hydraulic conductivity and the upward groundwater flow rate were estimated thanks to the combination of the measured and simulated chloride vertical profiles before injection. The tracer test experiment allowed us to validate these estimated values from the local vertical profile. The ERT time-lapse images (Fig. 7) helped to visualize the complex tracer infiltration and retrieval process, and to link the complex behaviour to the initial heterogeneous resistivity values of the studied zone (Fig. 3). However, due to uncertainties associated to the calculated resistivity values, we estimated that a statistical data treatment on ERT data, as in Ward *et al.* (2012), or a real coupling with the model, would have led to over-interpretation of this ERT data set.

Compared to studies performing Transient Storage Models (see Boano et al. (2014) and references therein), the data collection of this study was interrupted five hours after the injection, before full return to the initial state. This was observed in the last ERT image and last vertical chloride profile, both of which showed a persistent tracer signal within the less permeable HZ layer at the end of the monitoring. In the simulation, the relative mass change returned to a value lower than 1 % 11.8 hours after the beginning of the salt injection. Coming with this “incomplete monitoring”, the breakthrough curve within the river could not be correlated to a perfect salt mass budget. Indeed, the mixing within the river was not homogeneous, because of the very short distance between the injection and the monitoring site, imposed by the local configuration. Furthermore, the model selected relies upon very simplistic assumptions, neglecting the potential bank-storage processes, and heterogeneities across the width of the river. The focus was made on the mixing processes directly underneath the river, and they were assumed homogeneous on average: it means that the main features were supposed dominant compared to the small heterogeneities. The idea behind these simplifications was to highlight some of the major factors controlling the mixing rather than exactly replicate the field geometry and data.

Nevertheless, as the simplified 2D model was calibrated on vertically distributed chloride data, with a good fit for the initial state ($R^2 = 0.99$) and for the various time steps ($R^2 \geq 0.9$ except at t = 15’ and 35’ where the chloride concentration measured in the river was very low), it is assumed that a good understanding of the mixing processes has been achieved here, even without complete recovery data. The main contribution of this paper’s approach was to investigate the hydrodynamic parameters within the HZ, rather than precisely estimate the residence time. We were able to confirm the major character of the sediments’ hydraulic conductivity (with a highlighted vertical heterogeneity in this case) and the aquifer flow discharge towards the HZ to control the river flow infiltrating this interface.

These two crucial parameters were estimated with the help of vertically distributed chloride HZ data combined with a simplified physical multiprocess modelling. This study also confirmed the interest of using a physically based model for simulating the interaction between river and groundwater, as highlighted by Brunner et al. (2017). The ERT data allowed us to obtain the precise 2D distribution of the vertical heterogeneity in HZ hydraulic conductivity, as well as a 2D distribution of the tracer persistence within the HZ. This type of data was here also useful to visualize the distinct hydrodynamic behavior of the two characterized sediment layers.

## 5-Conclusion

In this paper, we described and used an approach combining field experimental and numerical tools to characterize solute exchanges within the HZ during an artificial tracer test experiment. In the field, the experiment was monitored with the help of tracer data (conductivity and sampling for chloride analysis collected from a multilevel HZ sampling device) and geophysical (ERT) methods. Surface and subsurface flows and tracer transport during the experiment were modelled with the HGS code.

The experimental data from the different methods are broadly consistent. The chloride plume monitored by chloride analysis and ERT profiles showed a 35 cm infiltration depth of the river water through the HZ.

Each experimental method allowed us to address some model uncertainties. The ERT measurements fixed one of the geomorphological uncertainties of the model: the ERT profile before tracer injection gave the location of the interface between the more resistive and permeable riverbed sediments and the conductive and less permeable clay layer at the bottom. The contrast in hydraulic conductivities was also observed with time-lapse ERT images, showing a rapid recovery of the initial state within the first layer, and a longer residence time of the tracer within the bottom layer. Chloride tracer was used as a robust target for fixing two other parameters of the modelling approach: the saturated hydraulic conductivity of this shallower and more conductive sediment layer and the groundwater flux that enters into the sediment at the bottom of the simulated domain. The estimation of the upward groundwater flow from simulated and measured natural chloride vertical profile before injection illustrated the interest of combining experimental approaches with physics-based models. The chloride field was demonstrated to be a good indicator of river conditions. The conclusion supported by field observations and by calibrated modelling is that the groundwater flux coming from the connected aquifer is essential to understand fully the solute transport in the surface and subsurface waters. This parameter could be here estimated thanks to the combination of the model and field data.

A clear contribution of modelling is to be able to simulate additional scenarios under different hydrological conditions. The sensitivity of the extension of the mixing zone to ambient groundwater flow conditions was studied. Three scenarios were considered: gaining, neutral, and losing river. Numerical simulations confirm the importance of groundwater discharge rate towards the river on the control of the HZ and mixing zone extension, and allow for the quantification of the residence time within the HZ.

Finally, we conclude that combining modelling with ERT and vertically distributed chloride sampling can resolve some of the uncertainties inherent in our understanding of transient storage and hyporheic exchange to date. It remains to be seen if such combined approaches are able to track the HZ behaviour under the influences of dynamic processes such as changes of the river water level.

## References

Boano F., Revelli R., & Ridolfi L. (2009), Quantifying the impact of groundwater discharge on the surface-subsurface exchange, *Hydrological processes*, *23 (15)*, pp. 2108-2116.

Boano F., Harvey J. W., Marion A., Packman A. I., Revelli R., Ridolfi L., & Wörman A. (2014), Hyporheic flow and transport processes: mechanisms, models, and biogeochemical implications, *Reviews of Geophysics*, *52*, pp. 603-679, doi: doi: 10.1002/2012RG000417.

Bouchez C., Cook P. G., Partington D., & Simmons C. T. (2021), Comparison of surface water-groundwater exchange fluxes derived from hydraulic and geochemical methods and a regional groundwater model, *Water Resources Research*, *57*, pp. e2020WR029137, doi: 10.1029/2020WR029137.

Brunner P., Therrien R., Renard P., Simmons C. T., & Franssen H.-J. H. (2017), Advances in understanding river-groundwater interactions, *Reviews of Geophysics*, *55*, pp. 818-854.

Buss S., Cai Z., Cardenas B., Fleckenstein J., Hannah D., Heppell K., . . . Wood P. (2009), The Hyporheic Handbook. A handbook on the groundwater-surface water interface and hyporheic zone for environment managers*, Environment Agency of England and Wales, Bristol, UK, Science Report SC050070*, 280 pp.

Cardenas M. B., & Wilson J. L. (2006), The influence of ambient groundwater discharge on exchange zone induced by curent-bedform interactions, *Journal of Hydrology*, *331*, pp. 103-109.

Cardenas M. B., & Wilson J. L. (2007), Hydrodynamics of coupled flow above and below a sediment-water interface with triangular bedforms, *Advances in Water Resources*, *30*, pp. 301-313.

Cardenas M. B. (2015), Hyporheic zone hydrologic science: a historical account of its emergence and a prospectus, *Water Resources Research*, *51*, pp. 3601-3616, doi: 10.1002/2015WR017028.

Castro N. M., & Hornberger G. M. (1991), Surface-subsurface water interactions in an alluviated mountain stream channel, *Water Resources Research*, *27 (7)*, pp. 1613-1621.

Cranswick R. H., Cook P. G., & Lamontagne S. (2014), Hyporheic zone exchange fluxes and residence times inferred from riverbed temperature and radon data, *Journal of Hydrology*, *519*, pp. 1870-1881.

Elliott A., & Brooks N. (1997), Transfer of nonsorbing solutes to a streambed with bed forms: theory, *Water Resources Research*, *33 (1)*, pp. 123-136.

Fox A., Boano F., & Arnon S. (2014), Impact of losing and gaining streamflow conditions on hyporheic exchange fluxes induced by dune-shaped bed forms, *Water Resources Research*, *50*, pp. 1895-1907, doi: 10.1002/2013WR014668.

Freeze R. A., & Cherry J. A. (1979), Groundwater*, Englewood Cliffs Eds., Prentice Hall,* 604 pp.

Harvey J. W., & Bencala K. E. (1993), The effect of streambed topography on surface-subsurface water exchange in mountain catchments, *Water Resources Research*, *29 (1)*, pp. 89-98.

Harvey J. W., Wagner B. J., & Bencala K. E. (1996), Evaluating the reliability of the stream tracer approach to characterize stream-subsurface water exchange, *Water Resources Research*, *32 (8)*, pp. 2441-2451.

Hester E., & Doyle M. (2008), In-stream geomorphic structures as drivers of hyporheic exchange, *Water Resources Research*, *44*, pp. W03417.

Houzé C. (2017), Etude des flux à l'interface nappe-rivière. Apport de l'outil hydrogéophysique couplé à des mesures hydrodynamiques, *PhD thesis, Université Paris Saclay, 253 pp*, https://tel.archives-ouvertes.fr/tel-01968020.

Houzé C., Durand V., Pessel M., & Ali T. (2017), Monitoring an artificial tracer test within streambed sediments with time lapse underwater 3D ERT, *Journal of applied Geophysics*, *139*, pp. 158-169.

Käser D. H., Binley A., Heathwaite L., & Krause S. (2009), Spatio-temporal variations of hyporheic flow in a riffle-step-pool sequence, *Hydrological processes*, *23*, pp. 2138-2149, doi: 10.1002/hyp.7317.

Kelleher C., Ward A., Knapp J. L. A., Blaen P. J., Kurz M. J., Drummond J. D., . . . Krause S. (2019), Exploring tracer information and model framework trade-offs to improve estimation of stream transient storage processes, *Water resources research*, *55 (4)*, pp. 3481-3501, doi: 10.1029/2018WR023585.

Lewandowski J., Arnon S., Banks E., Batelaan O., Betterle A., Broecker T., . . . Wu L. (2019), Is the hyporheic zone relevant beyond the scientific community?, *Water*, *11*, pp. 2230, doi: 10.3390/w11112230.

Loke M. H., & Barker R. D. (1996), Rapid least-squares inversion of apparent resistivity pseudosections by a quasi-Newton method, *Geophysical Prospecting*, *44*, pp. 131-152, doi: 10.1111/j.1365-2478.1996.tb00142.x.

McLachlan P. J., Chambers J. E., Uhlemann S. S., & Binley A. (2017), Geophysical characterisation of the groundwater–surface water interface, *Advances in Water Resources*, *109*, pp. 302-319, doi: 10.1016/j.advwatres.2017.09.016.

Munz M., Krause S., Tecklenburg C., & Binley A. (2011), Reducing monitoring gaps at the aquifer-river interface by modelling groundwater-surface water exchange flow patterns, *Hydrological processes*, *25*, pp. 3547-3562.

Rivett M. O., Ellis R., Greswell R. B., Ward R. S., Roche R. S., Cleverly M. G., . . . Dowle J. (2008), Cost-effective mini drive-point piezometers and multilevel samplers for monitoring the hyporheic zone, *Quarterly Journal Of Engineering Geology And Hydrogeology*, *41*, pp. 49-60.

Sawyer A. H., & Cardenas M. B. (2009), Hyporheic flow and residence time distributions in heterogeneous cross-bedded sediment, *Water Resources Research*, *45*, pp. W08406, doi: 10.1029/2008WR007632.

Schulze-Makuch D. (2005), Longitudinal dispersivity data and implications for scaling behaviour, *Ground Water*, *43 (3)*, pp. 443-456.

Su X., Yeh T.-C. J., Shu L., Li K., Brusseau M. L., Wang W., . . . Lu C. (2020), Scale issues and the effects of heterogeneity on the dune-induced hyporheic mixing, *Journal of Hydrology*, *590*, pp. 125429, doi: 10.1016/j.jhydrol.2020.125429.

Therrien R., Mclaren R. G., Sudicky E. A., & Park Y. J. (2012), HydroGeoSphere : A three-dimensional numerical model describing fully-integrated subsurface and surface flow and solute transport*, Groundwater Simulations Group, University of Waterloo*.

Tonina D., & Buffington J. M. (2007), Hyporheic exchange in gravel bed rivers with pool-riffle morphology: laboratory experiments and three-dimensional modeling, *Water Resources Research*, *43*, pp. W01421.

Triska F. J., Kennedy V. C., Avanzino R. J., Zellweger G. W., & Bencala K. E. (1989), Retention and transport of nutrients in a third-order stream in Northwestern California: hyporheic processes, *Ecology*, *70 (6)*, pp. 1893-1905.

Vernoux J.-F. (2001), Relations nappe-rivière et impact des prélèvements d'eau souterraine sur le débit des cours d'eau dans le bassin de la Juine et de l'Essonne*, BRGM, RP-50637-FR*, 80 pp.

Ward A. S., Gooseff M. N., & Singha K. (2010), Imaging hyporheic zone solute transport using electrical resistivity, *Hydrological processes*, *24*, pp. 948-953, doi: 10.1002/hyp.7672.

Ward A. S., Fitzgerald M., Gooseff M. N., Voltz T. J., Binley A. M., & Singha K. (2012), Hydrologic and geomorphic controls on hyporheic exchange during base flow recession in a headwater mountain stream, *Water Resources Research*, *48*, pp. W04513, doi: 10.1029/2011WR011461.

Ward A. S., Gooseff M. N., Fitzgerald M., Voltz T. J., & Singha K. (2014), Spatially distributed characterization of hyporheic solute transport during baseflow recession in a headwater mountain stream using electrical geophysical imaging, *Journal of Hydrology*, *517*, pp. 362-377.

Ward A. S. (2016), The evolution and state of interdisciplinary hyporheic research, *WIREs Water*, *3*, pp. 83-103, doi: 10.1002/wat2.1120.

Ward A. S., & Packman A. I. (2019), Advancing our predictive understanding of river corridor exchange, *WIREs Water*, *6 (1327)*, pp. 1-17, doi: 10.1002/wat2.1327.

Ward A. S., Wondzell S. M., Schmadel N. M., Herzog S., Zarnetske J. P., Baranov V., . . . Wisnoski N. I. (2019), Spatial and temporal variation in river corridor exchange across a 5th-order mountain stream network, *Hydrololy and Earth System Sciences*, *23*, pp. 5199-5225, doi: 10.5194/hess-23-5199-2019.

Woolhiser D. A. (1975), Simulation of unsteady overland flow, in *Unsteady Flow in Open Channels*, *Mahmood Eds., Fort Collins*.

## Figure captions

Figure 1. Location of the study area and important objects for the experiment

Figure 2. Chronology of all the measurements during the experiment

Figure 3. Reference ERT profile from West to East, before the injection; the distances are given in meters. The river is represented with the resistivity values that were taken into account as a constraint

Figure 4: Geometry and boundary conditions of the pseudo 2D model setup

Figure 5. Evolution of the water conductivity in the river before, during, and after injection of a salt solution in the river

Figure 6. Experimental vertical profiles of the chloride concentration in the pore water measured with the multi-sampling system before, during, and after injection. Error bars are equal to 5%. For clarity, they have only been added to one of the profiles.

Figure 7. Monitoring of ERT images expressed as percentage change in resistivity compared to the reference profile that was recorded before the beginning of the injection

Figure 8. Vertical profiles of the chloride concentration in the pore water before the tracer experiment. In each figure, symbols indicate measured data while the solid lines indicate modelled results obtained (a) with distinct values of the upper layer hydraulic conductivity, and (b) distinct values of the groundwater flux imposed at the bottom of the model domain

Figure 9. Simulated vertical profiles of the chloride concentration in the pore water obtained with the 2D model at the same place and at the same times as the observed values. In each figure, symbols indicate measured data while the solid lines indicate modelled results

Figure 10. Time evolution of the simulated chloride-transport fields under three different river conditions: gaining, neutral, and losing river. The three different conditions are imposed by changing the groundwater flux at the bottom boundary of the model domain. Steady-state flow directions are indicated at t=0 (arrows are of equal lengths and do not indicate magnitude)

Figure 11. Time evolutions of the relative mass change of chloride in the HZ for the three distinct river conditions: $F=10\times F_0$, $F=F_0$, and $F=-10\times F_{00}$

## *Appendix*

This Appendix gives a brief overview of the equations used to simulate the surface and subsurface flows and the transport in HGS.

The 2D surface water flow is modelled in HGS with the diffusion wave approximation of the Saint-Venant equations:

$$\frac{\partial d_0}{\partial t} + \boldsymbol{\nabla}. d_0\boldsymbol{u_0} = d_0\Gamma_0 Q_0 \qquad \text{(A-1)}$$

where $d_0$ is the flow depth [$L$], $\Gamma_0$ is the fluid exchange rate with the subsurface domain [$T^{-1}$], $Q_0$ is a volumetric flow rate per unit area representing external sources and sinks [$LT^{-1}$], and $\boldsymbol{u_0}$ is the surface fluid velocity [$LT^{-1}$] given by

$$\boldsymbol{u_0} = \frac{-{d_0}^{2/3}}{n\sqrt{S_f}}\boldsymbol{\nabla}(d_0 + z_l) \qquad \text{(A-2)}$$

In this expression, $n$ is the roughness Manning coefficient [$TL^{-1/3}$], $S_f$ is the friction slope [*dimensionless*], and $z_l$ is the bed or land surface elevation [$L$].

The 3D subsurface flows are modelled in HGS with the Richards' equation:

$$\frac{\partial \theta}{\partial t} + \boldsymbol{\nabla} \cdot \boldsymbol{u} = -\Gamma_0 Q \qquad \text{(A-3)}$$

where $\theta$ is the water content (dimensionless, $\theta = \theta_s S_w$ , where $\theta_s$ and $S_w$ are the porosity and the water saturation, respectively), $Q$ is the volumetric fluid flow per unit volume representing a source or a sink [$L^3\ L^{-3}T^{-1}$], and $\boldsymbol{u}$ is the subsurface Darcy velocity [$LT^{-1}$] given by

$$\boldsymbol{u} = -K. k_r\boldsymbol{\nabla}h \qquad \text{(A-4)}$$

In this expression, $K$ is the saturated hydraulic conductivity tensor [$LT^{-1}$], $k_r$ is the relative hydraulic conductivity of the medium [dimensionless], and $h$ is the subsurface water head [$L$].

HGS also solves the solute transport equations over the land surface and in the subsurface. The equation for 2D transport of solute along the surface domain is written as:

$$\frac{\partial}{\partial t}(d_0 C_0) + \boldsymbol{\nabla} \cdot (d_0 u_0 C_0 - d_0 D_0 \boldsymbol{\nabla} C_0) = -d_0 \Omega_0 \quad \text{(A-5)}$$

where $C_0$ is the solute concentration in surface water [$ML^{-3}$], $D_0$ is the hydrodynamic dispersion tensor of the surface flow domain [$L^2T^{-1}$], and $\Omega_0$ is the mass exchange rate of solutes per unit volume between the subsurface and the surface domain [$ML^{-3}T^{-1}$].

The 3D solute transport in the variably-saturated porous media is described by the following equation:

$$\frac{\partial}{\partial t}(\theta C) + \boldsymbol{\nabla} \cdot (\boldsymbol{u} C - \theta D \boldsymbol{\nabla} C) = \Omega_0 Q_c \quad \text{(A-6)}$$

where $C$ is the solute concentration in the subsurface domain [$ML^{-3}$], $D$ is the hydrodynamic dispersion tensor of the subsurface flow domain [$L^2T^{-1}$], and $Q_c$ represents a source or a sink term [$ML^{-3}T^{-1}$]. The hydrodynamic dispersion tensor $D$ [$L^2T^{-1}$] is given by Therrien et al. (2012):

$$\theta \boldsymbol{D} = (\alpha_l - \alpha_t)\frac{\boldsymbol{uu}}{|\boldsymbol{u}|} + \alpha_l |\boldsymbol{u}| \boldsymbol{I} + \theta \tau D_{free} \boldsymbol{I} \quad \text{(A-7)}$$

where $\alpha_l$ and $\alpha_t$ are the longitudinal and transverse dispersivities [$L$], respectively, $|\boldsymbol{u}|$ is the magnitude of the Darcy velocity, $\tau$ is the tortuosity [dimensionless], $D_{free}$ is the free solution diffusion coefficient [$L^2T^{-1}$] and $\boldsymbol{I}$ is the identity tensor.

In our pseudo 2D configuration where surface flow is only 1D, the hydrodynamic dispersion $D_o$ for the surface flow transport reduces to:

$$D_o = \alpha_{lo} |\boldsymbol{u}| + D_{free} \quad \text{(A-8)}$$